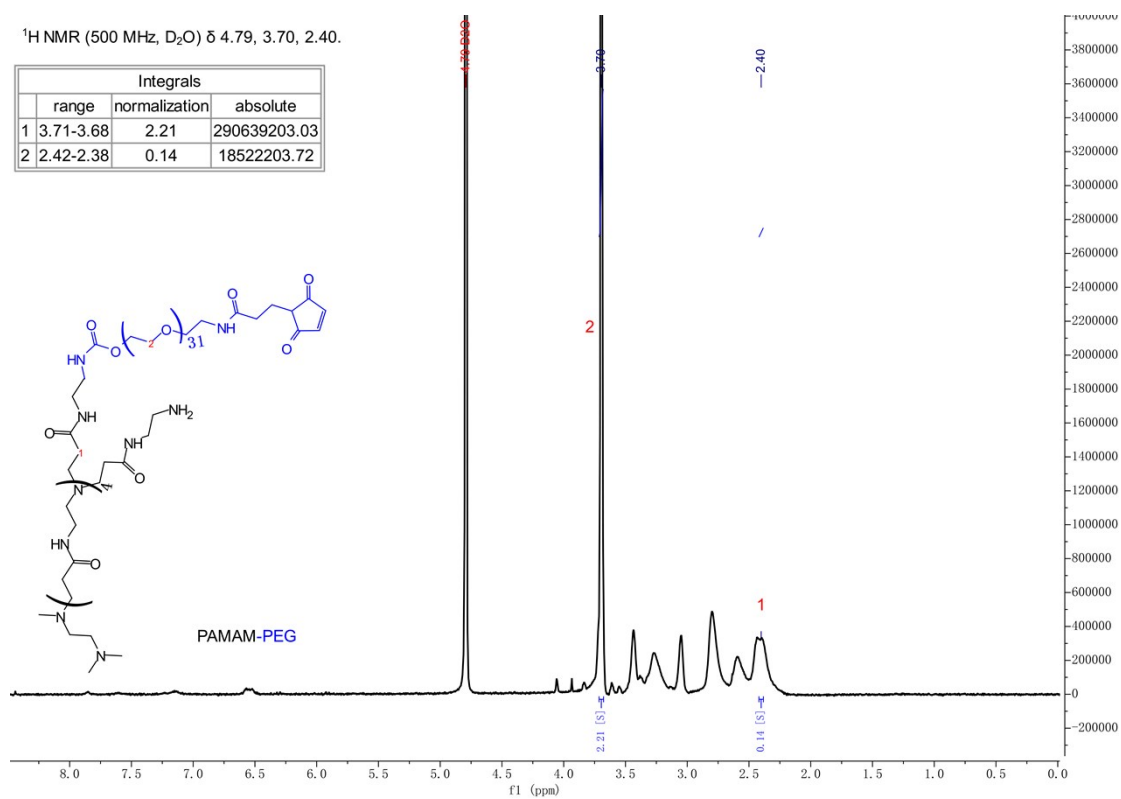


Supporting information



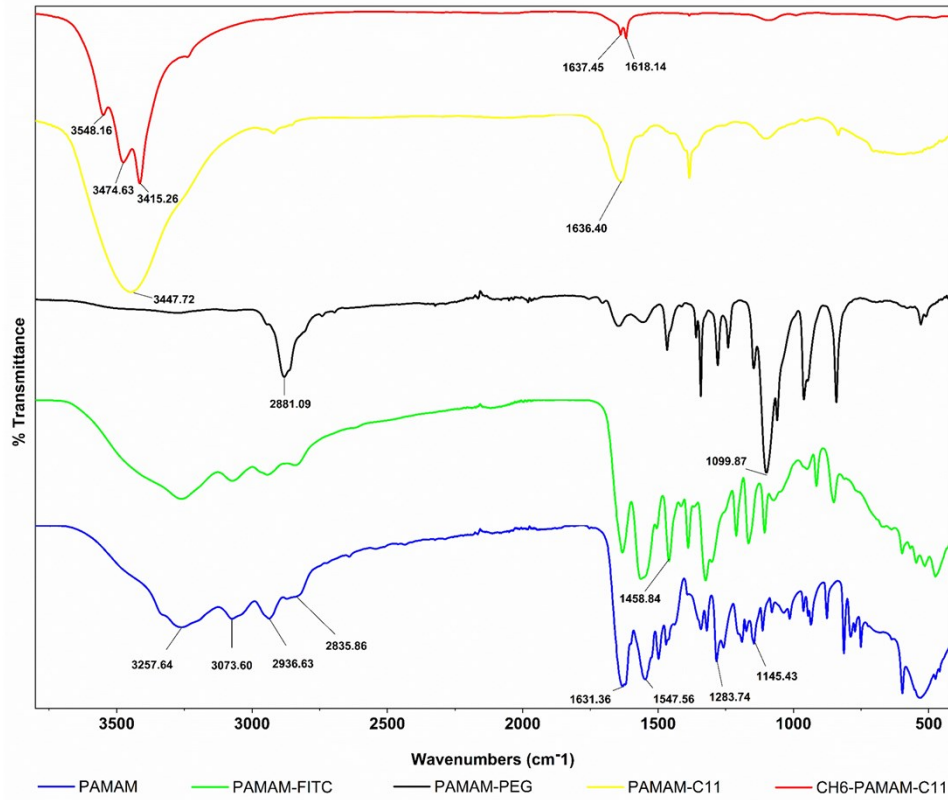


Figure S2. FTIR spectra of PAMAM, PAMAM-FITC, PAMAM-PEG, PAMAM-C11, and CH6-PAMAM-C11.

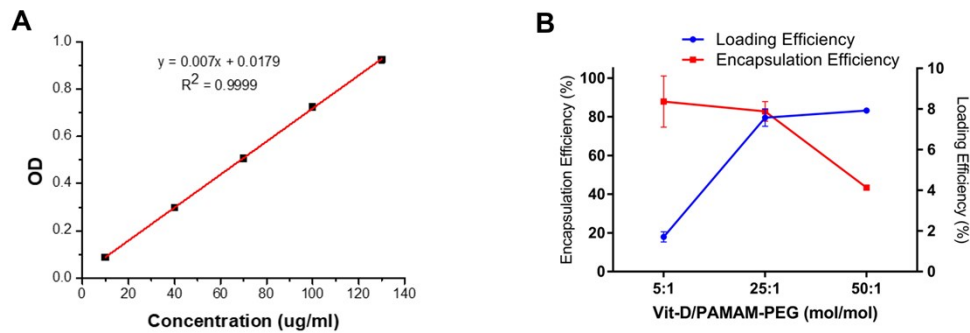


Figure S3. VitD loading of PAMAM-PEG. (A) Standard curve of VitD. (B) Encapsulation and loading efficiency of PAMAM-PEG for VitD at a VitD:PAMAM ratio of 5:1, 25:1, and 50:1. The results were obtained by measuring the absorbance of VitD and PAMAM-PEG in PBS solution containing 10% DMSO at 280 nm, and the data are reported as the mean \pm s.d. (n = 6).

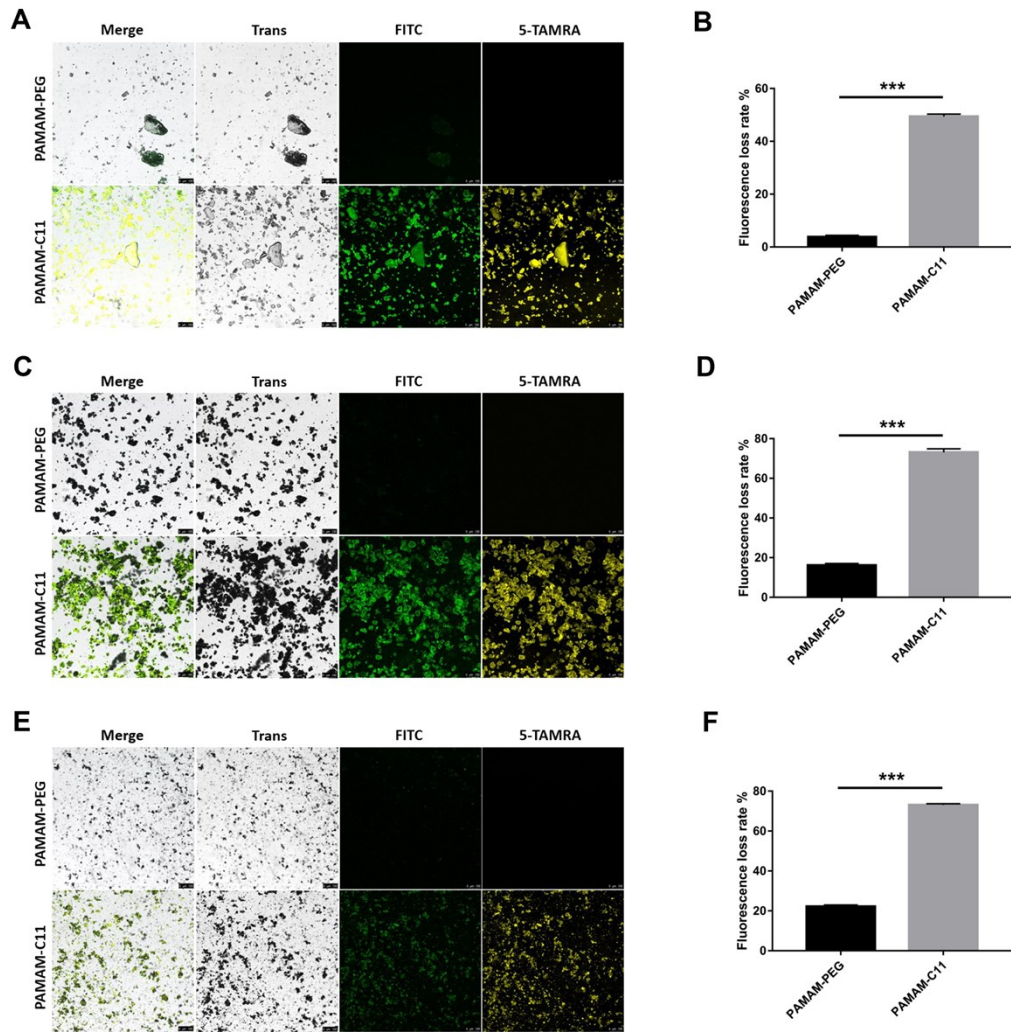


Figure S4. Binding to calcium-containing inorganics of PAMAM-C11. Representative confocal laser fluorescence images of HAP binding (A), Ca₃(PO₄)₂ binding (C), and CaC₂O₄ binding (E) of PAMAM-PEG and PAMAM-C11 nanocarriers. Colocalization of HAP (Trans) with FITC-labeled PAMAM dendrimer (green) and 5-TAMRA-labeled C11 peptide (yellow). HAP (50 μM) was stirred with 5 μg/ml nanocarrier alone for 1 h. Scale bars, 100 μm. Quantitative analysis of the FITC fluorescence loss rate determined by analyzing the supernatant of 5 μM HAP (B), Ca₃(PO₄)₂ (D), and CaC₂O₄ (F) stirred with 5 μg/ml nanocarrier alone for 1 h. ****P* < 0.001 by t-test. *n* = 3 per group. Data are the mean ± s.e.

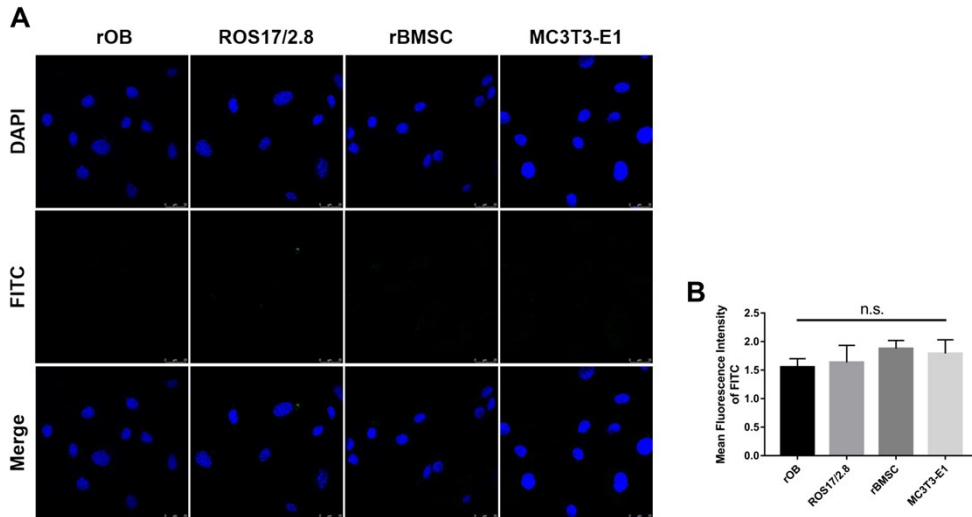


Figure S5. Cellular targeting of nanocarrier. (A) Representative confocal laser fluorescence images of cellular selectivity of FITC-labeled PAMAM-PEG for rat primary osteoblasts (rOBs), rat ROS 17/2.8 osteoblasts, rat bone marrow mesenchymal stem cells (rBMSCs) and mouse MC3T3-E1 preosteoblasts. Nuclei were counterstained with DAPI (blue). Scale bars, 25 μ m. (B) Quantitative analysis of the mean fluorescence intensity (FITC) of confocal images of cellular selectivity of PAMAM-PEG. No significance (n.s.) by t-test. $n = 3$ per group. Data are the mean \pm s.e.

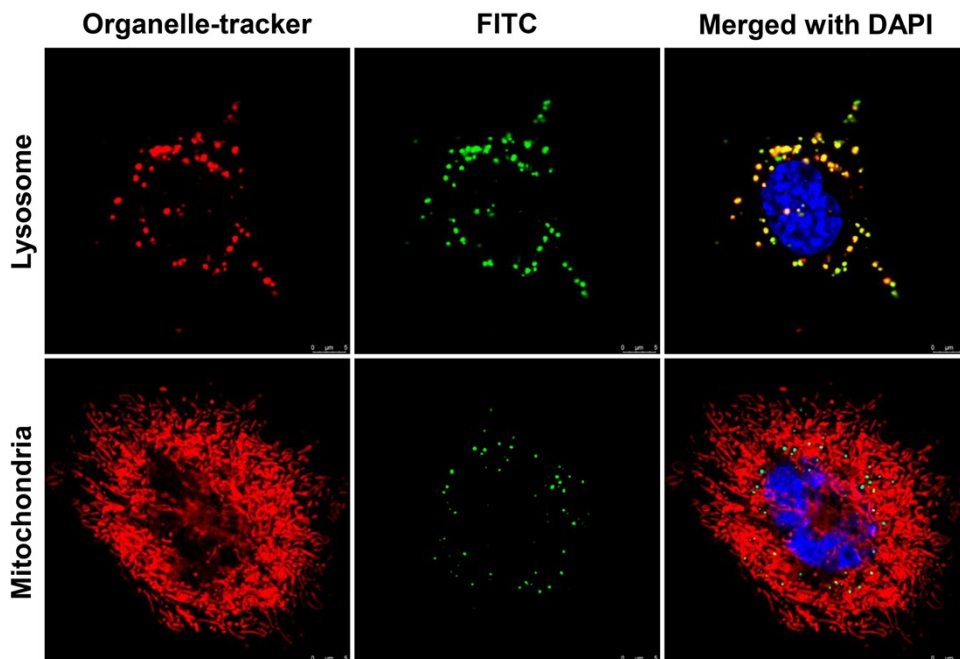


Figure S6. Cellular trafficking and subcellular localization of the PAMAM dendrimer. Lysosomal and mitochondrial colocalization in ROS 17/2.8 cells incubated with FITC-labeled PAMAM for 24 h. Cell nuclei were stained with DAPI. Lysosomes and mitochondria were stained by Lyso-Tracker Red and Mito-Tracker Deep Red FM, respectively. Scale bars, 5 μ m.

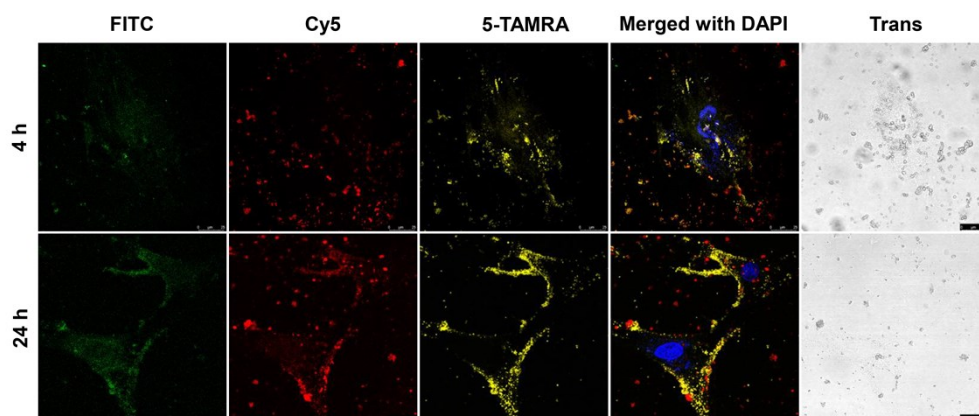


Figure S7. Selectivity of CH6-PAMAM-C11 nanocarriers for rOBs co-existed with HAP. Representative confocal fluorescence image of the selectivity of CH6-PAMAM-C11 for rOBs and HAP after co-culture 4 h and 24 h. rOBs were seeded on a substrate containing HAP 24 h in advance. Scale bars, 25 μm .



Figure S8. Extraction and identification of rOBs and rBMSCs. Optical (A) and microscopy images (B) of ALP staining of rOBs and rBMSCs cultured for 2 days without any inducers.

Table S1. The physicochemical characteristics of PAMAM, PAMAM-PEG, PAMAM-CH6, and CH6-PAMAM-C11 polyplexes. (data represent the mean \pm S.D., n=3)

polyplexes	Particle sizes		Zeta potential (mV)
	Z-average (nm)	Polydispersity index (P.D.I.)	
PAMAM	4.00 ± 0.57	0.19 ± 0.11	13.53 ± 2.44
PAMAM-PEG	12.22 ± 0.82	0.18 ± 0.01	3.94 ± 1.74
PAMAM-CH6	20.79 ± 1.40	0.15 ± 0.02	1.13 ± 1.40
CH6-PAMAM-C11	40.66 ± 3.77	0.25 ± 0.02	-1.15 ± 2.26

Table S2. Sequences and modifications of CH6 aptamer and C11 peptide.

Name	Sequences and modifications	Molecular weight
CH6	(5'-3') Cy5-AGTCTGTTGGACCGAATCCCGTGGACGCACCC- TTTGGACG-THS	13348
C11	(-N to -C) CSTDK(5-TAMRA)TKREEVD	1823